Benha Journal of Applied Sciences (BJAS) **print: ISSN 2356–9751**
Vol.(5) Issue(7) Part (2) (2020), (231-243) **online: ISSN 2356–976x**
http://bjas.journals.ekb.eg

Aminopyridine Transition Metals Complexes; Characterization, Application and Molecular Orbital Calculation

M. E. Moustafa[1], N. M. Meshal[1], M. I. Ayad[2]and O. A. Goda[1]
[1]Chemistry Department, Faculty of Science, Benha University, Benha, Egypt.
[2]Chemistry Department, Faculty of Science, Menofia University, Shiben El - kom, Egypt
E-mail: osamagoda55@yahoo.com

Abstract

Synthesis and characterization of nine complexes formed from the reaction of metal ion salts (chloride or acetate) of Mn^{2+}, Co^{2+}, Ni^{2+}, Cu^{2+}, Zn^{2+} and Cd^{2+} (I – IX) and 4-aminopyridine (4Am) with variable stoichiometric ratios were studied and their chemical structures were discussed. The prepared complexes were characterized by different chemical and physical techniques. The antimicrobial activity of the studied complexes was tested against representative bacteria and fungi. The results suggested the high - to - moderate activities against the tested organisms compared to ampicillin taken as a standard drug. The cytotoxic activities of some selected complexes were tested against *Lung carcinoma cells* A-549 cell line. The results obtained showed that the complexes are considered to have high to moderate activity. The catalytic activity of Ni(4AM) (1:4) complex was tested for the removal of orange G (OG^{+}) dye from waste water sample where almost complete removal of the dye was performed after 90 min. Molecular modeling and quantum chemical parameters of the Mn^{2+}, Co^{2+}, Ni^{2+} and Zn^{2+} complexes were studied and calculated. Also, the total density function, deformation density function and frontier orbital energy were determined using DFT method.

Keywords: 4–aminopyridine, transition metal complexes, biological and catalytic activities, molecular orbital calculation.

1. Introduction

During the last few decades, metals-based aminopyridinato complexes have attracted a tremendous research interest because of immense industrial needs for the catalyst which would be of higher activity and selectivity with lower toxicity and lower cost [1-4]. These types of complexes also found many biological and antitumor activities [5-8]. Although, some theoretical calculations were performed on the aminopyridine complexes [9,10] but no calculations were found using DFT theory. In the present work nine Mn^{2+}, Co^{2+}, Ni^{2+}, Cu^{2+}, Zn^{2+} and Cd^{2+} - 4-aminopyridine (4Am) complexes with variable stoichiometric ratios were prepared and their chemical structure were studied. The antibacterial and antitumor activities toward some bacteria, fungi and Lung carcinoma A-549 cell line were also studied. The catalytic activity of one complex for the removal of organic pollutant from waste water sample was tested. Molecular modeling and quantum chemical parameters of the complexes were studied and calculated. Also, the total density function, deformation density function and frontier orbital energy were determined using DFT method.

2. Experimental

All reagents used in the present study were of the highest quality (Merck, Aldrich, Fluka or Sigma Research Laboratories) and were used without further purification. Aqueous solution of 1.00 mmol of metal salts was added with stirring to an ethanolic solution of 4-aminopyridine ligand with the desired molar ratio. The mixture was refluxed for ≈ 6 hours then cooled to room temperature, and the solid complexes so formed were filtered off and washed with distilled water followed by ethanol and dried under vacuum.

2.1. Physical measurements

Elemental analysis; (C, H and N) of the mixed ligands complexes were carried out in the Regional Center for Mycology & Biotechnology, Al – Azhar University, Cairo, Egypt. Metal ion content (Mn, Ni, Co, Cu and Zn) was determined by EDTA titration under the appropriate conditions [11]. Infrared spectra of the complexes were recorded as KBr disc technique using FT – IR spectrometer Model Nicolet is 10-thermo-scientific within the wavenumber range 4000 – 400 cm^{-1}; Faculty of Science, Benha University. Thermogravimetric analysis were carried out using Shimadzu TGA – 50H thermal analyzer within the range 25 – 800 ºC under nitrogen atmosphere at heating rate of 10 ºC per minute at Central Lab, Faculty of Science, Menofia University, Shebin El-Kom, Egypt. The electronic absorption spectra in solid state (Nujol mull technique) were recorded on Jasco V – 530 (UV-Vis) double beam spectrophotometer (Japan) with scanning speed 400 nm/min and band width 2.0 nm. Magnetic moment values were measured at room temperature using a Sherwood scientific magnetic susceptibility balance. Molar conductivities of the complexes (10^{-3} M) in DMF were obtained using a conductivity bridge YSI model 32

2.2. Antimicrobial Screening

The antibacterial activity of some complexes toward some bacterial strains was evaluated by agar well diffusion method [12]. The tested complexes were dissolved in DMF to get concentration of 100 mg/ml. A hot nutrient agar solution (20 ml) was poured into the sterilized petri dishes and allowed to attain room temperature. The seed layer medium was melted and cooled to ≈ 45 ºC with gentle shaking. The previously

grown subculture was added to the seed layer medium aseptically and mixed well. It was immediately raked into the petri dishes and allowed to attain room temperature. Then wells were made with the sterile cork porer and to these wells, different concentrations (mgl/ml) of the tested complexes were added and the plates were allowed to cool for one hour to facilitate the diffusion. The plates were incubated at 37 ºC for 24 hours. Antibacterial activity of the complexes was evaluated by measuring the diameter of zone of inhibition in mm. The medium with DMF as solvent was used as a negative control whereas media with Ampicillin were screened separately for its standard antibacterial activity.

2.3. Antitumor activity assay

The cytotoxic effect of some complexes was tested against Lung carcinoma A-549 cell line. The work was performed as described in our previous work [13]. The relation between surviving cells and complex concentration was plotted to get the survival curve of each tumor cell line after treatment with the specified compound. The 50% inhibitory concentration (IC_{50}) was estimated from graphic plots of the dose response curve for each concentration [14,15]. All measurements were carried out at the Regional Center for Mycology and Biotecnology, Al-Azhar University, Cairo, Egypt.

2.4. The photocatalytic degradation

The photocatalytic activity was evaluated by the decomposition of malachite green (MG^+) in aqueous solutions under UV irradiation. A 20 W UV lamp (λ = 253.7 nm) was used as light source with light intensity of 0.75 mW/cm^2. The complex used as catalyst powder (20 mg) was added to 250 mL of MG^+ (30 mg/L). The distance between the liquid surface and the light source is kept at 10 cm and the solution was stirred for 5 min before irradiation. During the experiment the concentration of the dye and percent degradation were determined using a UV-visible spectrophotometer at its maximum wavelength (618 nm).

2.5. Molecular modeling

The cluster calculations using DMOL^3 program [16] in materials studio package [17] which is designed for the realization of large scale density functional theory calculation (DFT) were performed. DFT semi-core pseudopods calculations (dspp) were performed with the double numerica basis sets plus polarization functional (DNP). The DNP basis sets are of comparable quality to 6-31 G Gaussian basis sets [18].

3. Results and Discussion

1- Characterization of the metal complexes

The prepared complexes were suggested to have the following structural formulae:

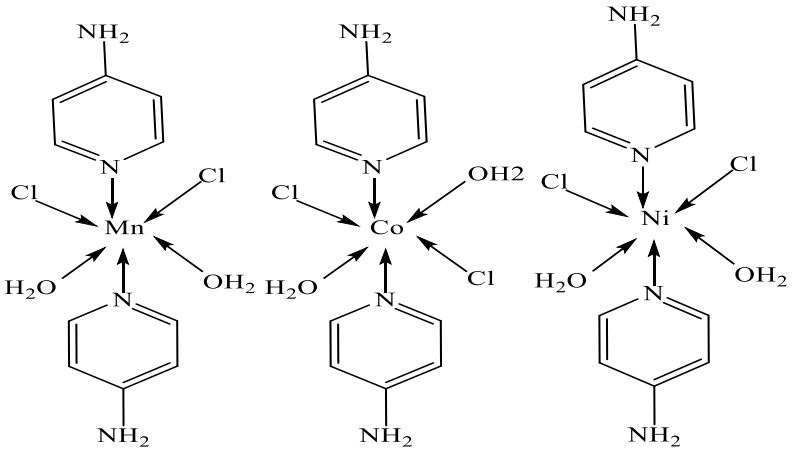

$MnCl_2$:4Am (1:2)(I) $CoCl_2$:4Am (1:2) (II) $NiCl_2$:4Am (1:2) (III)

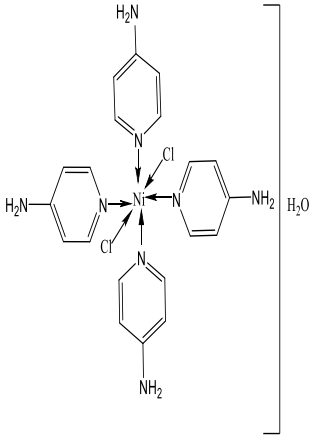

$NiCl_2$:4Am (1:4) (IV)

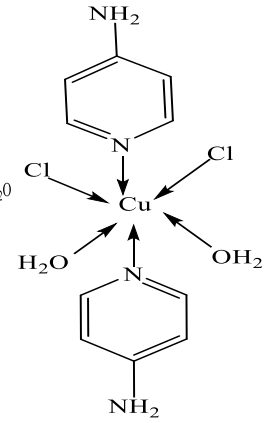

$CuCl_2$:4Am (1:2) (V)

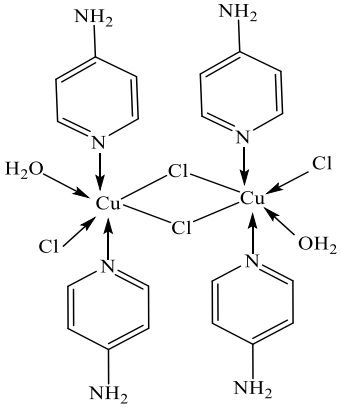

$CuCl_2$:4Am (1:2) (VI), dimer

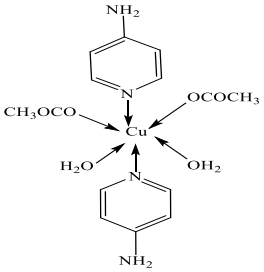

Cu(OAc)2:4Am (1:2) (VII)

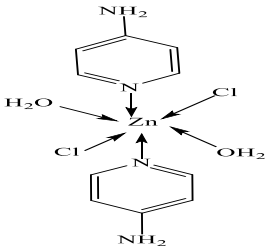

$ZnCl_2$:4Am (1:2) (VIII)

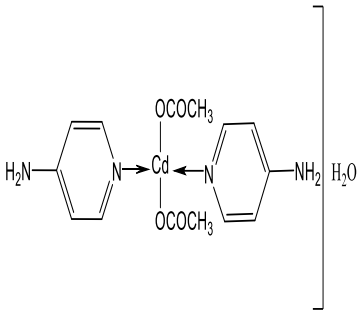

$Cd(OAc)_2$:4Am (1:2) (IX)

i- Elemental analysis and molar conductivity

All the complexes are colored, stable in air and have high melting points (> 300 °C). They are freely soluble in DMSO and DMF but sparingly soluble in other common organic solvents. Results of elemental analysis (Table 1) are in good agreement with the calculated values of the proposed formulae in accordance with the stoichiometric ratio. The molar conductance values of the complexes lie within the range 9.12 - 11.47 $ohm^{-1} cm^2 mol^{-1}$ indicating their nonionic nature. The presence of the counter anion (Cl^-) inside the coordination sphere is confirmed by the not precipitation of Cl^- as AgCl by the addition of $AgNO_3$ solution to the solubilized chelates in DMF.

Table (1): Elemental analysis and molar conductivity data of the complexes.

Complex	Tentative formula	M.Wt.	Elemental analysis*				Λ_m^{**}
			%C	%H	%N	%M	
$MnCl_2$:4Am (1:2)(I)	$C_{10}H_{16}N_4O_2Cl_2Mn$	349.00	34.32 (34.38)	4.57 (4.62)	16 (16.05)	15.7 (15.74)	10.21
$CoCl_2$:4Am (1:2) (II)	$C_{10}H_{16}N_4O_2Cl_2Co$	353.00	33.93 (33.99)	4.52 (4.57)	15.83 (15.87)	16.65 (16.70)	9.12
$NiCl_2$:4Am (1:2) (III)	$C_{10}H_{16}N_4O_2Cl_2Ni$	353.86	43.14 (33.94)	4.52 (4.56)	15.84 (15.83)	16.59 (16.59)	11.05
$NiCl_2$:4Am (1:4) (IV)	$C_{20}H_{26}N_8OCl_2Ni$	524.08	45.85 (45.84)	4.69 (5.00)	21.38 (21.38)	11.2 (11.20)	11.47
$CuCl_2$:4Am (1:2) (V)	$C_{10}H_{16}N_4O_2Cl_2Cu$	358.5	33.5 (33.61)	4.46 (4.52)	15.62 (15.69)	17.72 (17.63)	10.54

$CuCl_2$:4Am (1:2)(VI), dimer	$C_{20}H_{28}N_8O_2Cl_4Cu_2$,	681.15	35.26 (35.25)	4.11 (4.14)	16.45 (16.44)	18.65 (18.65)	9.88
$Cu(Ac)_2$:4Am(1:2)(VII)	$C_{14}H_{22}N_4O_6Cu$	405.90	41.44 (41.43)	5.42 (5.46)	13.8 (13.80)	15.66 (15.66)	10.68
$ZnCl_2$:4Am (1:2) (VIII)	$C_{10}H_{16}N_4O_2\ Cl_2\ Zn$	360.7	33.29 (33.52)	4.43 (4.50)	15.53 (15.65)	18.25 (17.86)	9.08
$Cd(Ac)_2$:4Am(1:2) (IX)	$C_{14}H_{20}N_4O_5Cd$,	436.75	38.51 (38.50)	4.58 (4.62)	12.83 (12.83)	25.74 (25.74)	9.45

*values between parentheses are found values ** $ohm^{-1}\ cm^2\ mol^{-1}$.

ii- Thermal analysis

The prepared metal ion complexes degrade thermally within the temperature range 33.4 ºC – 800.0 ºC through, more or less, three main steps as summarized numerically in Table (2). The first step within the temperature range 64 – 179 ºC corresponds to the removal of physically adsorbed and coordinated water molecules from the coordination sphere, respectively. This step appears, sometimes as a composite one. The unhydrated solid complex begins to decompose thermally through the second step started at 336.6 ºC and ended at 498.5 ºC, in which CO_2, N_2 gases are evolved. Full thermal decomposition takes place through the third step at temperature higher than 332 ºC leading to metal oxides as final products. The overall weight losses of the degradation steps were calculated (***c.f.*** Table 2) and the metallic residues were determined.

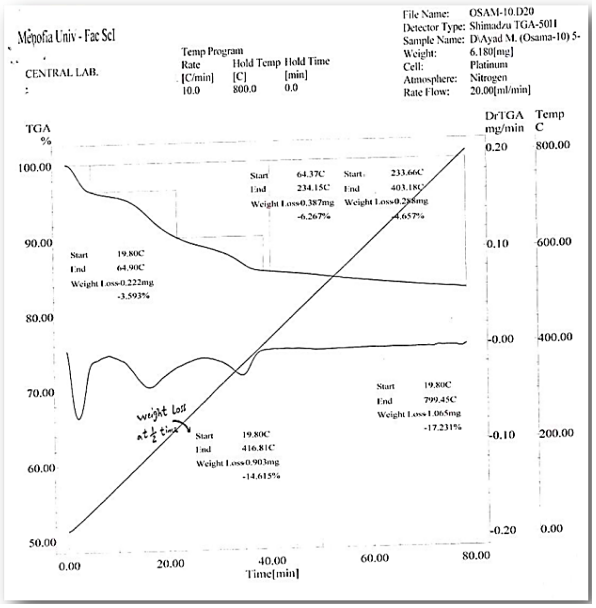

Fig (1): TGA and Dr TGA curves of $MnCl_2$:4Am (1:2) complex (I).

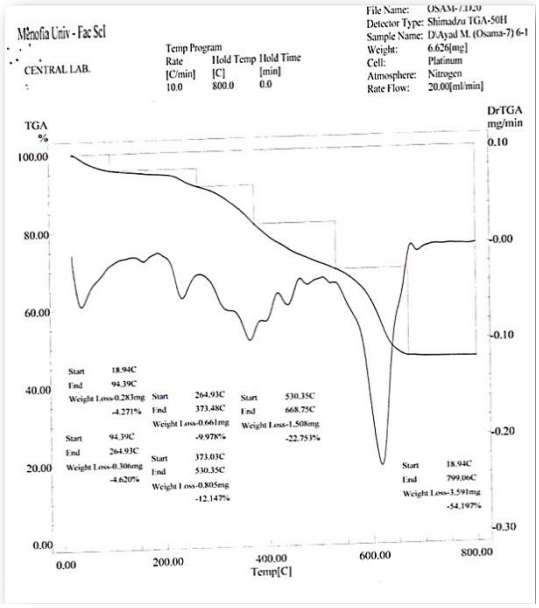

Fig (2): TGA and Dr TGA curves of $CoCl_2$:4Am (1:2) (II) complex.

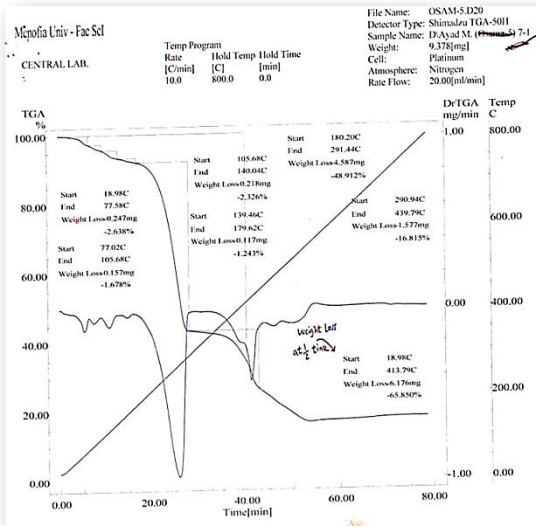

Fig (3): TGA and Dr TGA curves of $NiCl_2$:4Am (1:4) (IV) complex.

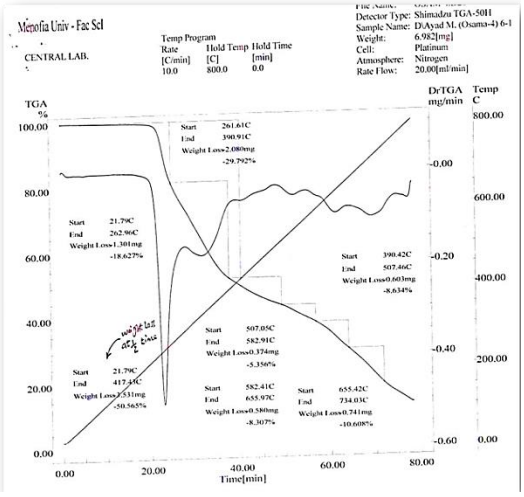

Fig (4): TGA and Dr TGA curves of $CuCl_2$:4Am (1:2) (V) complex.

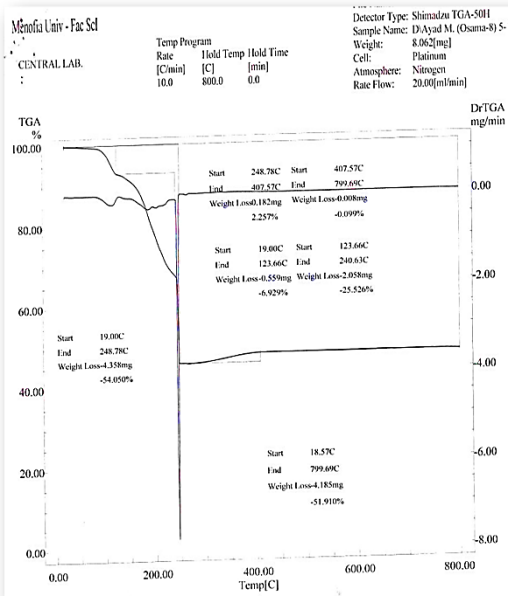

Fig (5): TGA and Dr TGA curves of $Cu(Ac)_2$:4Am(1:1)(VII) complex.

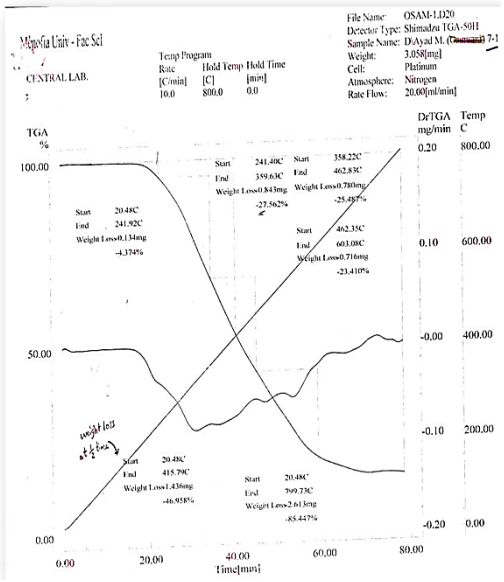

Fig (6): TGA and Dr TGA curves of $ZnCl_2$:4Am (1:2) (VIII) complex.

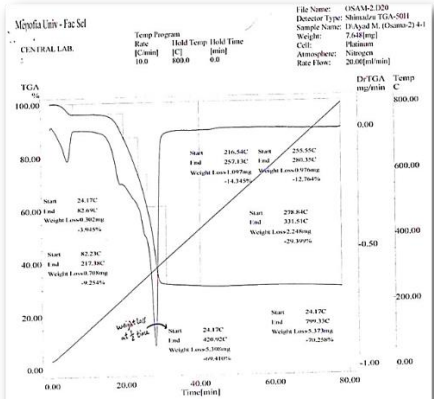

Fig (7): TGA and Dr TGA curves of

$Cd(Ac)_2$:4Am(1:2) (IX) complex.

Table (2): Thermogravimetric data of the metal complexes with 4-aminopyidine.

Complex	Decomposition Temp(°C)	% W.t Loss	Assignment
$MnCl_2$:4Am	19.80-64.90	3.59	Removal of physically adsorbed water
(1:2)(I)	64.37-234.15	6.27	Removal of coordinated water, HCl gas
	233.66-403.18	4.66	Decomposition of the organic moiety
Overall	19.80-799.45	17.23	
$CoCl_2$:4Am	18.94-94.39	4.27	Removal of physically adsorbed water
(1:2) (II)	94.39-264.93	4.62	Removal of coordinated water
	264.93-373.48	9.98	Starting decomposition of complex
	273.03-530.35	12.15	Evolving of gaseous fragments
	530.35-668.75	22.75	Final decomposition of complex to CoO
overall	18.94-799.06	54.20	
$NiCl_2$:4Am	77.58-105.68	4.32	Removal of physically adsorbed water
(1:4) (IV)	105.68-140.04	2.33	Removal of coordinated water
	139.46-179.62	1.24	Starting decomposition of complex
	180.20-291.44	48.91	Evolving of gaseous fragments
	290.94-439.79	16.81	Final decomposition of complex to NiO
overall	18.98-439.79	65.85	
$CuCl_2$:4Am	21.79-417.43	50.57	Removal of coordinated water
(1:2) (V)	582.41-655.97	8.31	Starting decomposition of complex, HCl gas
	655.42-734.03	10.61	Final decomposition of complex to CuO
Overall	21.79-734.02	69.49	
$Cu(Ac)_2$:4Am	19.00-248.78	54.05	Removal of coordinated water
(1:1)(VII)	248.78-407.57	2.26	Starting decomposition of complex, HCl gas
	407.57-799.00	0.10	Final decomposition of complex to CuO
Overall	18.57-799.69	51.91	
$ZnCl_2$:4Am	20.48-241.92	4.37	Removal of adsorbed and coordinated water
(1:2) (VIII)	241.40-359.63	27.26	Starting decomposition of complex
	358.22-462.83	25.49	Evolving of gaseous fragments
	462.35-603.03	23.41	Final decomposition of complex to ZnO
overall	20.48-799.73	85.45	
$Cd(Ac)_2$:4Am	82.23-217.38	13.95	Removal of adsorbed and coordinated water
(1:2) (IX)	216.54-257.13	14.35	Starting decomposition of complex
	255.55-280.35	12.76	Evolving of gaseous fragments
	278.84-331.51	29.40	Final decomposition of complex to CdO
Overall	24.71-799.33	70.26	

iii- Infrared spectra

The IR spectra of the complexes M ← 4-aminopyridine were studied and correlated to their molecular structure. The absorption band frequencies are listed in Table (3) which shows that the spectra exhibit broad band within the range 3405 – 3519 cm^{-1} and weak band within the range 2965 – 3033 cm^{-1} due to the stretching vibrations of OH and NH_2 (V_{OH} and V_{NH2}) groups, respectively. These bands suffer notable broadness and shifting to lower frequencies indicating their contribution in coordination process. This is accompanied by the presence of new broad bands within the range 3400 – 3350 cm^{-1} and 584 – 545 cm^{-1} due to the stretching vibrations of coordinated water molecules and the stretching vibration of M – O bond, respectively. The stretching vibration of the C=N group ($V_{C=N}$) in the 4-aminopyridine moiety appears at 1550 - 1690 cm^{-1} range while that of the stretching vibration of the C-N group (V_{C-N}) appears at 1416 - 1535 cm^{-1} range. The OH in – plane deformation of the coordinated water molecules gives rise to band within the range 1003 – 1130 cm^{-1}. The out – of – plane deformation of the OH group of the complexes is represented by the strong band within the range 852 – 740 cm^{-1}, while the far infrared region of the spectra of the metal chelates shows new sets of bands within the region 570 – 658 and 403 - 603 cm^{-1} which are due to M – Cl and M – N bonds, respectively.

Table (3): IR vibrational frequencies (cm^{-1}) of some function groups of Mn^{2+}, Zn^{2+}, Co^{2+}, Ni^{2+}, Cu^{2+} and Cd^{2+} complexes with 4-aminopyridine.

Complex	V_{OH}	V_{NH2}	$V_{C=N}$	V_{C-N}	δ_{OH}	V_{M-Cl}	V_{M-N}
$MnCl_2$:4Am (1:2)(I)	3405	2967	1653	1531	1101	575	508
$CoCl_2$:4Am (1:2) (II)	3553	2965	1634	1522	1098	725	521
$NiCl_2$:4Am (1:2) (III)	3405	2968	1653	1531	1102	629	508
$NiCl_2$:4Am (1:4) (IV)	3440	2912	1633	1521	1110	573	523
$CuCl_2$:4Am (1:2) (V)	3429	3215	1616	1584	1130	653	537
$CuCl_2$:4Am (1:2)(VI), dimer	3398	3024	1551	1416	1021	658	487
$Cu(Ac)_2$:4Am(1:2)(VII)	3519	3024	1550	1416	1021	658	403
$ZnCl_2$:4Am (1:2) (VIII)	3440	3224	1633	1521	1024	573	523
$Cd(Ac)_2$:4Am(1:2) (IX)	3443	3033	1690	1535	1003	670	603

iii- Electronic absorption spectra and magnetic properties

The electronic absorption spectra of the complexes are studied in solid state (using Nujol mull technique) and the electronic absorption bands are expressed in terms of wavenumber (cm^{-1}). The spectral data are given in Table (4). Inspection of the data obtained shows that:

- The high spin Mn (II) complexes with d^5 configuration have the ground state $^6A_{1g}$ and all d-d transitions are spin and laporte forbidden (as represented by Tanabe – Sugano diagram). All. Complexes of Mn^{2+} are colorless or faint pink. The electronic spectra display different weak bands as listed numerically in Table (4), the most important of them are assignable to $^6A_{1g}(S) \rightarrow {}^4T_{1g}(G)$, $^6A_{1g}(S) \rightarrow {}^4T_{2g}(G)$ and $^6A_{1g}(S) \rightarrow {}^4E_g, {}^4A_{1g}(G)$ transitions indicating that the complex possesses a high spin octahedral configuration [19].

- The electronic absorption spectrum of Co(II) complex in shows bands at 33333.33, 30303.03 and 27027.03 cm^{-1} due to (d - d) transitions of the types $^4T_{1g(F)} \rightarrow {}^4T_{1g(P)}$ (V_3), $^4T_{1g(F)} \rightarrow {}^4A_{2g(F)}$ (V_1) and $^4T_{1g(F)} \rightarrow {}^4T_{2g(F)}$ (V_2), respectively [20]. The use of Tanabo - Sugan diagram for the spin allowed electronic transition in d^7 configuration was used to calculate the crystal field splitting energy (10Dq), Racah parameters **B**, β and crystal field stabilization energy.

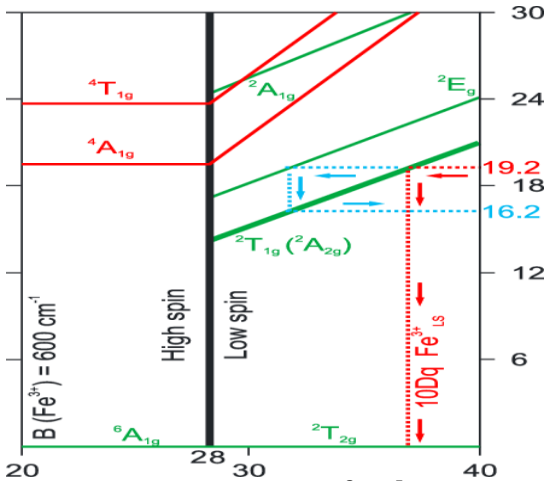

Tanabe – Sugano diagram for Mn^{2+} (d^5) configuration

- From Tanabe – Sugano diagram of d^8 configuration, the ground state term is $^3A_{2g(F)}$ with only three spin allowed excited states, namely; $^3T_{1g(P)}$, $^3T_{1g(F)}$ and $^3T_{2g(F)}$. Other transitions are both spin forbidden and/or Laporte forbidden. So, the electronic absorption spectrum of Ni (II) (d^8) complex shows the three spin allowed bands at 33444.82, 28985.51 and 23809.52cm^{-1} which are assigned to electronic transition type $^3A_{2g(F)} \rightarrow {}^3T_{1g(P)}$, $^3A_{2g(F)} \rightarrow {}^3T_{1g(F)}$ and $^3A_{2g(F)} \rightarrow {}^3T_{2g(F)}$ respectively.

` Copper (II) d^9 complexes have ^2D spectral term. The transition is from the $(t_{2g})^6(e_g)^3$ configuration (^2E_g state) to the $(t_{2g})^5(e_g)^4$ configuration ($^2T_{2g}$ state). This could also be described as a positive "hole" that moves from the e_g to the t_{2g} orbital set. The sign of Dq is opposite that for d^1, with a ^2E_g ground state and a $^2T_{2g}$ excited state. Like the d^1 case, d^9 octahedral complexes do not require the Tanabe–Sugano diagram to predict their absorption spectra [21].

- Zn (II) and Cd(II) complexes (d^{10} configuration) have no d – d electron transitions because the d orbitals are completely filled. Thus, UV-VIS absorption bands are not observed the absorption bands in their spectra are due to n→π* or CT interaction. The spectral data are fully assigned in Table (4).

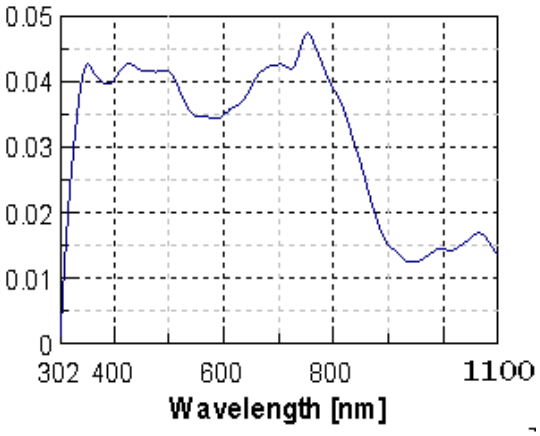

Electronic absorption spectra of Mn^{2+}-4-aminopyridine complex in Nujol mull.

Table (4): Spectral data of the complexes in Nojol mull.

Complex	Nojol mull		Assignment
	λ_{max} (nm)	Wavenumber (cm^{-1})	
Mn^{2+}	650 725 1080	15384.62 13793.10 9259.30	$^6A_{1g}(S) \rightarrow {}^4T_{1g}(G)$, $\rightarrow {}^4T_{2g}(G)$ $\rightarrow {}^4E_g, {}^4A_{1g}(G)$
Co^{2+}	300 330 370sh	33333.33 30303.03 27027.03	$^4T_{1g(F)} \rightarrow {}^4A_{2g(F)}(\nu_2)$ $\rightarrow {}^4T_{1g(P)}(\nu_3)$ $\rightarrow {}^4T_{2g(F)}(\nu_1)$
Ni^{2+}	299 345sh 420sh	33444.82 28985.51 23809.52	$^3A_{2g(F)} \rightarrow {}^3T_{1g(P)}(\nu_3)$ $\rightarrow {}^3T_{1g(F)}(\nu_2)$ $\rightarrow {}^3T_{2g(F)}(\nu_1)$
Cu^{2+}	305 345sh	32786.89 28985.51	 $^2a_{1g(D)} \rightarrow {}^2b_{1g(D)}$ $^2e_{g(D)} \rightarrow {}^2b_{1g(D)}$

Calculation of the spectral data

From the electronic absorption spectra and by the use of Tanabe-Sugano diagrams, the values of crystal field splitting energy (Δ_o), Racah parameter (B), nephelauxetic ratio (β) and the crystal field stabilization energy can be determined. For Co (II) complexes (d^7) the diagram shows three spin-allowed transitions (V_1, V_2 and V_3). In order to determine the Racah parameter (B) and Δ, the following steps are followed:

- The position on the horizontal axis (Δ/B) where the ratio between the lines representing V_2/V_1 is determined, then a vertical line is drawn at this position.
- The value on the vertical axis (E/B) that corresponding to the spin-allowed transitions is found so as to determine V_1/B, V_2/B and V_3/B.
- Knowing the values of V_1, V_2 and V_3 the values of B and Δ can be calculated.
- The crystal field stabilization energy is calculated from the equation:

$CFSE = (-0.6 \times nt_{2g} + 0.4 \times n_{eg}) \times \Delta$

- The nephelauxetic ratio (β) is given by $\beta = B'/B$..

From the β values, the covalence factor ($b^{1/2}$), Sinha parameter (δ %) (metal – ligand covalency percent) and the covalency angular overlap parameter (η) have been calculated using the relations [22, 23]:

$b^{1/2} = 1/2[(1 - \beta)^{1/2}]$, $\delta\ \% = [[(1 - \beta)/\beta]x100$ and $\eta = (1 - \beta)^{1/2} / \beta^{1/2}$ The spectral parameters of Co(II) and Ni(II) complexes are given in Table (5)

Table (5): Spectral parameters of Co(II) and Ni(II) complexes.

Complex	Spectral parameters					
	Δ_o (cm^{-1})	B' (cm^{-1})	B	%δ	H	CFST (cm^{-1})
Co(II)complexes	17448	759	0.69	44.93	0.670	-13958
Ni(II) complexes	18787	606	0.58	71.53	0.846	-22544

Magnetic Susceptibility

Magnetic susceptibility measurements at room temperature exhibit paramagnetism for Mn(II), Ni(II) and Cu(II) complexes and diamagnetism for Zn(II) and Cd(II) complexes as expected. The μ_{eff} values, term symbols and ground state symbols are listed in Table (6).

Table (6.): Magnetic properties of the prepared complexes.

Complex	d^n	Electronic configuration	Term symbol	Ground State	μ_{eff} (BM)	
					Found	Theor.
$MnCl_2$:4Am (1:2)(I)	d^5	$t_{2g}^3e_g^2$	$^6S_{5/2}$	$^6A_{1g}(S)$	5.41	5.477
$CoCl_2$:4Am (1:2) (II)	d^7	$t_{2g}^6e_g^1$	$^4F_{9/2}$	^4F	4.01	3.464
$NiCl_2$:4Am (1:2) (III)	d^8	$t_{2g}^6e_g^2$	$^3F_4$	$^3A_{2g}$	2.78	2.450
$NiCl_2$:4Am (1:4) (IV)	d^8	$t_{2g}^6e_g^2$	$^3F_4$	$^3A_{2g}$	2.91	2.450
$CuCl_2$:4Am (1:2) (V)	d^9	$t_{2g}^3e_g^3$	$^2D_{5/2}$	^2E_g	1.79	1.732
$CuCl_2$:4Am (1:2)(VI), dimer	d^9	$t_{2g}^6e_g^3$	$^2D_{5/2}$	^2E_g	1.73	1.732
$Cu(Ac)_2$:4Am(1:2)(VII)	d^9	$t_{2g}^6e_g^3$	$^2D_{5/2}$	^2E_g	1.80	1.732
$ZnCl_2$:4Am (1:2) (VIII)	d^{10}	$t_{2g}^6e_g^4$	$^1S_0$		Dia	0.00
$Cd(Ac)_2$:4Am(1:2) (IX)	d^{10}	$t_{2g}^6e_g^4$	$^1S_0$		Dia	0.00

iv- Electron Spin resonance (ESR) spectra

The X-Band ESR spectra of the powder Cu(OAC)2 ← 4-amnopyridine and CuCl2← 4-aminopyridine (1:2) complexes (*c.f.* Fig. 1) were recorded at room temperature using DPPH as reference standard. The ESR spectra of the complexes show anisotropic spectra with $g_{II} > g_{\perp} > g_e$ ***(c.f.*** *Table 7)* characteristic for compressed axial symmetry of the coordination sphere (one coordination axis (*z*) is significantly shorter than the other two (*x*, *y*) with d_{x2-y2} ground state. One unpaired electron in Cu (II) complex with $^2B_{1g}$ as ground state lies in d_{z2} orbital and follows the trend $g_{\perp} > g_{II} > g_e$ (g_e = 2.0036 free ion value). Analysis of spectra gave the g_{II} and $g_{\perp}$ values as cited in Table (7.).

Table (7): ESR spectral parameters for Cu(II) complexes.

Complex	g_{II}	$g_{\perp}$	g_{av}
$Cu(OAC)_2$ ← 4-amnopyridine	2.09069	2.15974	2.13672
$CuCl_2$← 4-aminopyridine	2.1006	2.13619	2.12433

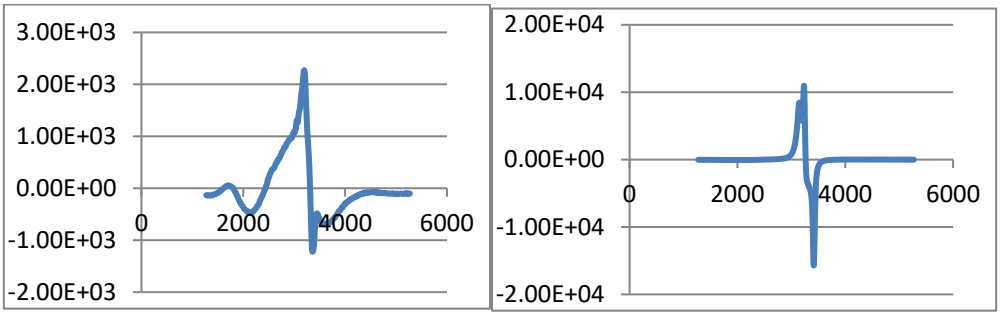

Fig (1): ESR spectra of the complex $Cu(OAC)_2$ ← 4-amnopyridine (A) and the complex $Cu(Cl)_2$ ← 4-amnopyridine (B).

Biological activity

The antimicrobial and antifungal activities of selected representative complexes is tested against two bacterial; ***Staph.aureus***, ***E.coli*** and two fungi; ***Asper.ocherationus***, ***Asper.niger*** species. Standard drug; Ampicillin and DMF solvent control were screened separately for their antibacterial activity. The results (*c.f.* Table 8) suggest that the complexes show a moderate activity against the tested organisms compared to Ampicillin taken as a standard drug. Also, percent Activity Index data show that Zn (II) complexes have the highest activity followed by Cu (II), Mn (II) and finally Co (IV) complexes.

Table (8): Antibacterial and antifungal activities of some complexes in terms of inhibition zone diameter (mm) and % activity index.

Organism	***Bacteria***				***Fungi***			
Complex	***Staph.aureus***		***E.coli***		***Asper.ocherationus***		***Asper.niger***	
	Inh.zone, mm	% Ac.Ind	Inh.zon, mm"	% Ac.Ind	Inh.zone "mm"	% Ac.Ind	Inh.zone "mm"	% Ac.Ind
Ampicillin	15	100	20	100	20	100	20	100
DMF	10.33	68.87	18.33	91.65	19.68	98.40	19.69	98.40
$CuCL_2$ + 4-aminopyridine " 1:4"	10.00	66.67	14.67	73.00	18.35	91.75	8.67	43.35
$CuCL_2$ + 4-aminopyridine " 1:2"	10.67	70.67	13.67	68.00	20.37	101.85	10.53	52.65
$ZnCL_2$ + 4-aminopyridine " 1:2"	19.67	130.67	15.00	75.00	19.00	95.00	0.00	0.00
$MnCL_2$ + 4-aminopyridine " 1:2"	12.00	80.00	16.33	81.65	13.38	66.90	0.00	0.00
$NiCL_2$ + 4-aminopyridine " 1:2"	10.00	66.67	11.67	58.35	13.75	67.50	0.00	0.00
$CoCL_2$ + 4-aminopyridine "1:2"	0.00	0.00	14.67	73.35	20.33	101.65	0.00	0.00

Antitumor activity

The cytotoxic activities of some selected complexes were tested against ***Lung carcinoma cells* A-549 cell line** and compared to that of Vinblastine as a standard drug. The relation between surviving cells and complex concentration is plotted to get the survival curve of each tumor cell line after treatment with the tested complexes. The 50% inhibitory concentration was estimated from graphic plots of the dose response curve for each concentration. The lethal concentrations (IC_{50}) values with a brief comment on the data are listed in Table (9).

Table (9): Lethal concentration (IC_{50}) of the complexes against Lung carcinoma.

Complex	IC_{50} (µg/ml), comment
Vinblastine	4.6
{$MnCl_2$&4-amino "1:2"}	***Weak inhibitory activity against Lung carcinoma cells was detected under the experimental conditions with IC_{50} = >500 µg/ml.***
{$NiCl_2$&4-amino "1:4"}	***Moderate activity against Lung carcinoma cells was detected under the experimental conditions with IC_{50} = 28.5 ± 0.6 µg/ml.***
{$CoCl_2$&4-amino }	***Very high activity against Lung carcinoma cells was detected under the experimental conditions with IC_{50} =6.94 ± 0.2 µg/ml.***
{$CuCl_2$&4-amino "1:2"}	***Moderate activity against Lung carcinoma cells was detected under the experimental conditions with IC_{50} = 59.4± 0.9 µg/ml.***
$ZnCl_2$ – 4-amino (1:2)	***Weak inhibitory activity against Lung carcinoma cells was detected under the experimental conditions with IC_{50} = >500 µg/ml.***
{$Cd(OAC)_2$&4-amino "1:2"}	***Weak inhibitory activity against Lung carcinoma cells was detected under the experimental conditions with IC_{50} = >500 µg/ml.***

From the data cited in the Table, it is clear that $CoCl_2$ complexes showed very high activity toward lung carcinoma cell with a very low IC_{50} value (6.94 µg/ml) while Cu(II) and Ni(II) complexes showed moderate activities. On the other hand, other tested complexes showed weak activities against the tested cell line.

Photocatalytic degradation of Organic G dye

The photodegradation efficiency of the complex; $NiCl_2$:4Am (1:4) (IV) was tested using Orange G (OG) as model. The percent degradation efficiency (%D) was calculated from which it was found that the absorbance decreases and the photodegradation efficiency increases (reaching a plateau) as a function of time (Fig 2). The results showed that the maximum percent of degradation of OG dye was about 80% after 90 min in case of UV illumination in the presence of hydrogen peroxide and complex IV as catalyst indicating the very high catalytic efficiency of this complex.

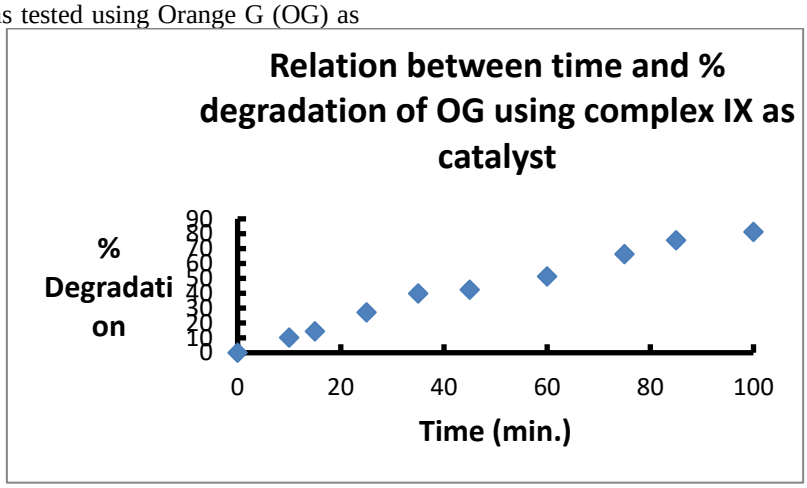

Fig (2): Effect of time on the % degradation of OG using complex IV as catalyst

Analysis of kinetic data

The kinetic of the removal process was treated in terms of pseodo 1st and 2nd order models. Applying the mathematical relations of both models showed that the pseudo first order model is the better applicable

Molecular orbital calculations

A group of measurements involving DMOL[3] program in materials studio package which is shaped for the recognized of wide scale Density Function Theory (DFT) were applied. The molecular modeling and total density using DFT method for the complexes $MnCl_2$:4Am (1:2)(I), $NiCl_2$:4Am (1:2) (III), $NiCl_2$:4Am (1:4) (IV), $ZnCl_2$:4Am (1:2) (VIII) and $Cd(Ac)_2$:4Am (1:2) (IX) were determined and given, representatively, in Fig.'s (3 and 4). All the bond lengths and bond angles and bond lengths were also calculated.

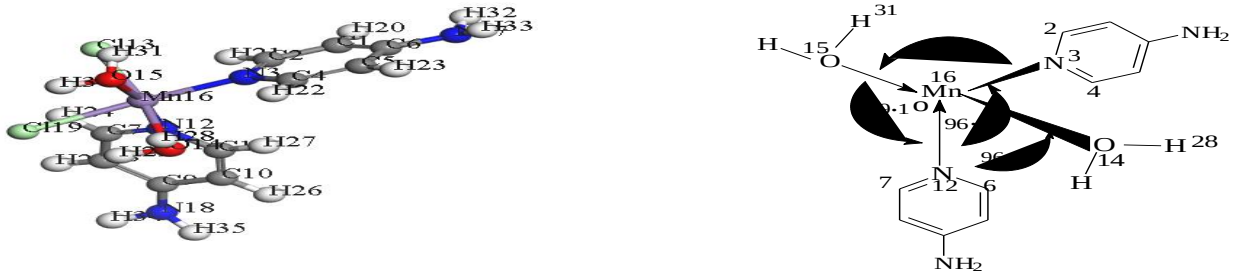

Fig (3) : Molecular modeling of $MnCl_2$:4Am (1:2)(I)complex

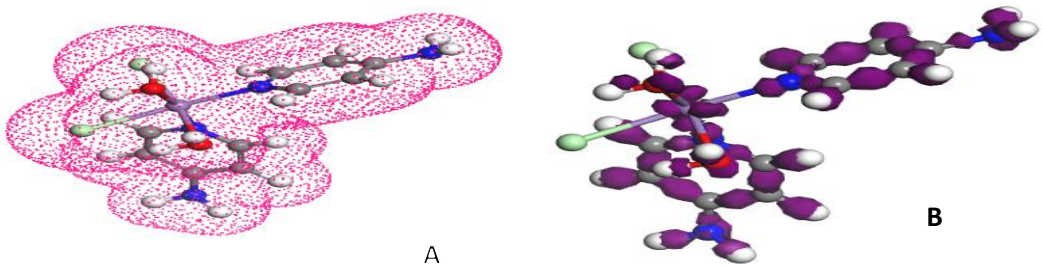

Fig (4): Total density (A) and Deformation density (B) using DFT method for of $MnCl_2$:4Am (1:2)(I)complex

Frontier molecular orbitals

The HOMO's and LUMO's are known as Frontier molecular orbitals (FMOs), which played an important role for evaluating molecular chemical stability, chemical reactivity and hardness-softness of the molecule [24]. The HOMO and LUMO energy, energy gap (ΔE), absolute electronegativity (χ) Chemical hardness (η), softness(σ) and electrophilicity index (ω) [25,26] values are listed in Table 10. Picture of Frontier Molecular Orbitals and Deformation Density is shown, representatively, in Fig.(5).The energy gap (ΔE) represents the chemical reactivity of compounds. For a system lower value of ΔE makes it more reactive or less stable. As depicted in Table 10, Cd← 4-aminopyridine complex has a largest energy gap (2.383 ev) which decreases in the following order Mn← 4-aminopyridine (0.1.318 eV) > Ni← 4-aminopyridine (1:4) (0.902 eV) > Ni← 4-aminopyridine **(1:2)** (0.665 eV) > Zn← 4-aminopyridine (0.247eV). Thus complex Cd← 4-aminopyridine referred as hard molecule when compared to other complexes [27]. Another global reactivity descriptor electrophilicity index (ω) describes the electron accepting ability of the systems quite similar to hardness and chemical potential. High values of electrophilicity index increases electron accepting abilities of the molecules.

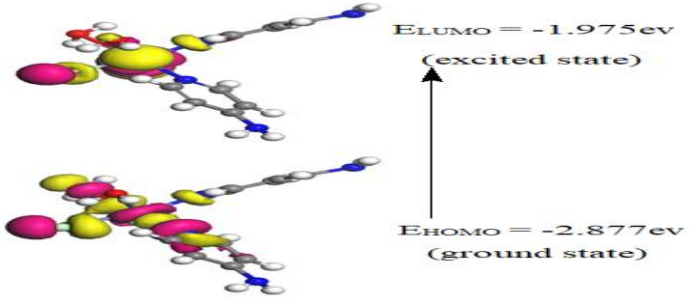

Fig (5): 3D plots frontier orbital energies using DFT method for $NiCl_2$:4Am (1:2) (III) complex.

The electrophilicity index (ω) is positive, definite quantity and the direction of the charge transfer is completely determined by the electronic chemical potential (μ) of the molecule because an electrophile is a chemical species capable of accepting electrons from the environment and its energy must decrease upon accepting electroic charge. Therefore, the electronic chemical potential must be negative exactly as supported by the values in Table 11. The values of (E_{HOMO}-E_{LOMO}) energies of frontier molecular orbitals, energy band gap that explains the final charge transfer interaction inside the molecule, electronegativity (χ), chemical potential (μ), global hardness (η), global softness (σ), additional electronic charge (ΔN_{max}) and global electrophilicity index (ω) were calculated and listed in Table (11):

$\chi = -1/2\ (E_{LUMO}+E_{HOMO})$

$\mu = -\chi = 1/2\ (E_{LUMO}+E_{HOMO})$

$\eta = 1/2\ (E_{LUMO}-E_{HOMO})$

$\Delta N_{max} = -\mu / \eta \qquad \omega = \mu^2/2\ \eta$

The inverse value of the global hardness is designed as the softness (σ); $\sigma = 1/\eta$.

Table (10): The calculated quantum chemical parameters of the complexes

Complex	HOMO	LUMO	ΔE	H	Σ	X	M	ω	ΔNmax
$MnCl_2$:4Am (1:2) (I)	-2.729	-1.411	1.318	0.659	1.517450683	-2.07	2.07	3.251062215	3.141122914
$NiCl_2$:4Am (1:2) (III)	-2.607	-1.9418	0.6652	0.3326	3.006614552	-2.2744	2.2744	7.776451233	6.838244137
$NiCl_2$:4Am (1:4) (IV)	-2.877	-1.975	0.902	0.451	2.2172949	-2.426	2.426	6.52491796	5.379157428
$ZnCl_2$:4Am (1:2) (VIII)	-3.145	-2.898	0.247	0.1235	8.097165992	-3.0215	3.0215	36.96138563	24.46558704
$Cd(Ac)_2$:4Am (1:2) (IX)	-4.142	-1.759	2.383	1.1915	0.839278221	-2.9505	2.9505	3.653147398	2.47629039

Table (11): Some energetic properties of the complexes calculated by DFT-method

Complex	Eenergy components (Kcal/mol)						Binding energy (Kcal/mol)
	Sum of atomic energies	Kinetic energy	Electrostatic energy	Exchange-correlation energy	Spin polarization energy	Total energy	
$MnCl_2$:4Am (I)	$-1.128\ X10^6$	-582.44	$-5.506X10^3$	$1.324\ X10^3$	$1.322\ X10^3$	$-1.131\ X10^6$	$-4.345\ X10^3$
$NiCl_2$:4Am (III)	$-1.456\ X10^6$	$-2.015X10^3$	$-8.410\ X10^3$	$2.477\ X10^3$	$2.030X10^3$	$-1.462\ X10^6$	$-5.918\ X10^3$
$NiCl_2$:4Am (IV)	$-1.173\ X10^6$	$-1.441X10^3$	$-4.829\ X10^3$	$1.486\ X10^3$	$1.232\ X10^3$	$-1.176\ X10^6$	$-3.552\ X10^3$
$ZnCl_2$:4Am(VII)	$-1.210\ X10^6$	$-1.709X10^3$	$-3.727\ X10^3$	$1.213\ X10^3$	$1.205\ X10^3$	$-1.214\ X10^6$	$-3.019\ X10^3$
$Cd(Ac)_2$:4Am(X)	$-7.202\ X10^6$	$-3.976X10^3$	$-3.624X10^3$	$1.829\ X10^3$	$1.426\ X10^3$	$-1.155\ X10^6$	$-4.345\ X10^3$

References

[1] M. Hafeez, M. Riaz, Aminopyridine stabilized group-IV metal complexes and their applications. Appl. Petrochem.l Res. B, Vol.6(4), PP.307–340, 2016.

[2] M. I. Baena, M. C. Marquez, V. Matres, J. Botella, A. Ventosa, Bactericidal Activity of Copper and Niobium–Alloyed Austenitic Stainless Steel. Curr. Microbiol. Vol.53(6), PP.491-495, 2006.

[3] P. Mialane, L. Tchertanov, F. Banse, J. Sainton, J. J. Girerd, Aminopyridine iron catecholate complexes as models for intradiol catechol dioxygenases. Synthesis, structure, reactivity, and spectroscopic studies. J. Inorg. Chem. Vol.39(12), PP.2440-2444, 2000.

[4] R. Huang, A. Wallqvist, G. Covell, Anticancer metal compounds in NCI's tumor-screening database: putative mode of action. Biochem. Pharmacol.Vol.69(7), PP.1009-1039, 2005.

[5] D. K. Demertzi, Recent advances on non-steroidal anti-inflammatory drugs, NSAIDs: Organotin complexes of NSAIDs. J. Organomet. Chem. Vol.691(8), PP.1767–1774, 2006.

[6] L. Mei, T. Haiming, L. Q. Rong, S. Jie, Y. S. Zhong, L. Liang, The synthesis of N-Zn, N-Cu complexes

involving 2-amino pyridine and ethylenediamine ligands and application to the Henry reaction. J. Chem. Sci. Vol.121(4), PP.435-440, 2009.

[7] C. R. Kowol, R. Trondl, V. B. Arion, M. A. Jakupec, I. Lichtscheidlb, B. K. Keppler, Fluorescence properties and cellular distribution of the investigational anticancer drugTriapine (3-aminopyridine-2-carboxaldehyde thiosemicarbazone) and its zinc(ii) complex. J. Dalton Trans. Vol.39(3), PP.704–706, 2010.

[8] N. V. Tkachenko, O. Y. Lyakin, D. G. Samsonenko, E. P. Talsi, K. P. Bryliakov, Highly efficient asymmetric aerobic oxidative coupling of 2-naphthols in the presence of bioinspired iron aminopyridine complexes. J. Catal. Commun. Vol.104(10), PP.112-117, 2018.

[9] U. Koch, P. L. A. Popelier, Characterization of C-H-O Hydrogen Bonds on the Basis of the Charge Density. J. Phys. Chem. Vol.99(24), PP.6387-6400, 1995.

[10] X. wang, D. sheng yang, Bonding and structures of copper-aminopyridine complexes — High-resolution electron spectroscopy and ab initio calculations. Can. J. Chem. Vol.87(1), PP.297-306, 2009.

[11] A. I. Vogel; "A Text Book of Quantitative inorganic analysis", Longmans, London, 1994.

[12] I. Ahmad, A. Z. Beg, Antimicrobial and phytochemical studies on 45 Indian medicinal plants against multi-drug resistant human pathogens. J. Ethanopharmacology. Vol.74(2), PP.113-123, 2001.

[13] I. M. I. Moustafa, S. M. Mabrouk, H. E. Megahed, M. A. Mohamed Photocatalytic Removal of Organic Pollutants from Industrial Wastewater Using MnO, NiO and Mixed MnO-NiO NP's as Catalyst. Int. J. Nano Med. Eng. Vol.4(6), PP.46-55, 2019.

[14] S. M. Gomha, S. M. Riyadh, E. A. Mahmmoud, M. M. Elaasser, Synthesis and Anticancer Activities of Thiazoles, 1,3-Thiazines, and Thiazolidine Using Chitosan-Grafted-Poly(vinylpyridine) as Basic Catalyst. Heterocycles. Vol.91(6), PP.1227-1243, 2015.

[15] T. Mosmann, Rapid colorimetric assay for cellular growth and survival: application to proliferation and cytotoxicity assays. J. Immunol. Methods. Vol.65(2), PP.55-63, 1983.

[16] B. Delley, Hardness conserving semilocal pseudopotentials. Phys. Rev. B : Condens. Matter. Vol.66(18), PP.125-155, 2002.

[17] In: Materials Studio, Accelrys software Inc.San Diego, USA, 2011.

[18] W. J. Hehre; Ab initio molecular orbital theory, Wiley-Interscience, 1986.

[19] U. G. Pranita, P. R. Mandlik, A. S. Aswar, Synthesis and Characterization of Cr(III), Mn(III), Fe(III), VO(IV), Zr(IV) and UO2(VI) Complexes of Schiff Base Derived from Isonicotinoyl Hydrazone. Ind. J. Pharm. Sci. Vol.77(4), PP.376-381, 2015.

[20] P. Kopel, Z. Travnicek, L. Kvitek, M. Biler, M. Pay licek, Z. Sindelar, J. Marek, Coordination compounds of nickel with trithiocyannic acid. Part IV Trans. Met. Chem. Vol.26(3), PP.282 – 286, 2001.

[21] S. A. Shaker, Y. Farina, S. Mahmoud, M. Eskender, Co(II), Ni(II), Cu(II) and Zn(II) mixed ligand complexes of 6-aminopurine, theophylline and thiocyanate ion, preparation and spectroscopic characterization. ARPN J. Eng. Appl. Sci. Vol.4(9), PP.1-3, 2009.

[22] M. Shebl, S. M. E. Khalil, S. A. Ahmed, H. A. A. Medien, Synthesis, spectroscopic characterization and antimicrobial activity of mono-, bi-and tri-nuclear metal complexes of a new Schiff base ligand. J. Mol. Struc. Vol.980(3), PP.39-50, 2010.

[23] A. A. Nejo, G. A. Kolawole, A. O. Nejo, Synthesis, characterization, antibacterial, and thermal studies of unsymmetrical Schiff-base complexes of cobalt(II). J. Coord. Chem. Vol.63(24), PP.4398–4410, 2010.

[24] E. E. Porchelvi, S. Muthu, Vibrational spectra, molecular structure, natural bond orbital, first order hyperpolarizability, thermodynamic analysis and normal coordinate analysis of Salicylaldehyde p-methylphenylthiosemicarbazone by density functional method. Spectrochimica Acta Part A: Molecular Spectroscopy. Vol.134(1), PP.453-464, 2015.

[25] M. S. Masoud, A. E. Ali, M. A. Shaker, G. S. Elasala, Synthesis, computational, spectroscopic, thermal and antimicrobial activity studies on some metal-urate complexes. Spectrochim. Acta A. Vol.90(8), PP.93-108, 2012.

[26] T. A. Yousef, O. A. El-Gammal, S. F. Ahmed, G. M. Abu El-Reash, Synthesis, biological and comparative DFT studies on Ni(II) complexes of NO and NOS donor ligands. Spectrochimica Acta Part A: Molecular and Biomolecular Spectroscopy. Vol.135(4), PP.690-703, 2015.

[27] R. R. Ternavisk, A. J. Camargo, F. B. C. Machado, J. A. F. F. Rocco, G. L. B. Aquino, V. H. C. Silva, H. B. Napolitano, Synthesis, characterization, and computational study of a new dimethoxy-chalcone. J. Mol. Mod. Vol.20(1), PP.2526-2528, 2014.